
**Showcasing research from the State Key Laboratory of High Power Semiconductor Lasers, School of Science, Changchun University of Science and Technology, Changchun, China, and the Department of Electrical and Electronic Engineering, Southern University of Science and Technology, Shenzhen, Guangdong, China.**

Linear and nonlinear optical characteristics of all-inorganic perovskite $CsPbBr_3$ quantum dots modified by hydrophobic zeolites

Hydrophobic zeolites were proposed for $CsPbBr_3$ quantum dots to prevent degradation by water molecules, while achieving good dispersion. This nanocomposite shows low defect degree, which results in improved optical performance. This strategy is universal and would be of great importance for both fundamental physics and practical applications.

## As featured in:

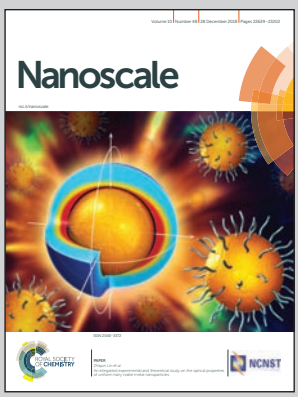


See Zhipeng Wei, Rui Chen *et al.*, *Nanoscale*, 2018, **10**, 22766.

ROYAL SOCIETY OF CHEMISTRY

rsc.li/nanoscale

Registered charity number: 207890

Nanoscale

PAPER



Cite this: *Nanoscale*, 2018, **10**, 22766

# Linear and nonlinear optical characteristics of all-inorganic perovskite $CsPbBr_3$ quantum dots modified by hydrophobic zeolites†

Ruxue Li,[a,b] Zhipeng Wei,*[a] Haixia Zhao,[a] Hongrui Yu,[a] Xuan Fang,[a] Dan Fang,[a] Junzi Li,[c] Tingchao He,[c] Rui Chen*[b] and Xiaohua Wang[a]

Received 6th September 2018,
Accepted 19th September 2018

DOI: 10.1039/c8nr07256f

rsc.li/nanoscale

All-inorganic perovskite quantum dots (QDs) have been considered as outstanding candidates for high-performance optoelectronic device applications. However, the chemical and optical stabilities restrict their device applications. In this paper, hydrophobic zeolites were proposed to modify $CsPbBr_3$ QDs to prevent water influence while achieving good dispersion. These hybrid luminescent materials possess high internal quantum efficiency (IQE, ~81%@3.52 W $cm^{-2}$) and low dissociation levels that give rise to improved optical stability in terms of temperature and time. More interesting, it is found that this nanocomposite is able to maintain its optical limiting performance under intensive laser illumination. This paper discusses the linear and nonlinear optical characteristics of $CsPbBr_3$ QDs, which would be of great importance for both fundamental physics investigation and practical multiphoton applications.

## 1 Introduction

Halide perovskites have attracted researchers' intensive attentions due to their strikingly high light-harvesting efficiency in photovoltaics in the past several years.[1,2] Compared with traditional semiconductor nanocrystals, perovskite nanocrystals exhibit excellent optical properties which manifest superb performance in electrically driven light-emitting diodes and optically pumped lasers.[3–7] Very recently, all-inorganic colloidal nanocrystals of cesium lead halide perovskites ($CsPbX_3$, X = Cl, Br, I) with high photoluminescence (PL) quantum yield (QY) up to 90% have been synthesized.[8,9] Among them, the all-inorganic perovskite $CsPbBr_3$ quantum dots (QDs) have been recognized as advantageous luminescent materials due to their large absorption cross-section and high exciton binding energy.[3,4] Though both the hybrid and all-inorganic perovskite QDs are reported to possess excellent optical properties, the latter ones exhibit better stability and most of the attention has been paid to them.[3] However, compared to the classical chalcogenide QDs, all-inorganic perovskite QDs are highly ionic in nature and sensitive to many polar solvents, especially water and moisture.[5,10,11] Therefore, the structural and optical stabilities of the material are the most important issues for practical applications of this new kind of functional material.

Many strategies have been proposed to solve the problems,[12] such as encapsulating perovskite QDs by organic or inorganic materials.[3,13–18] However, surface coating of thick shells around the QDs will influence their performance as luminescent materials, electrical injection and light extraction. Moreover, it has been reported that photo-induced regrowth of perovskite QDs will result in relatively lower PL QY, which is due to the decrease of exciton binding energy and the increase of defects. Therefore, the perovskite QDs also need good dispersion in order to achieve high optical performance. It has been proposed that mesoporous silica could be a protective shell for perovskite QDs and was beneficial to improve their dispersibility.[19,20] But, this strategy only considered the dispersibility of the QDs, while the waterproof property was ignored.

Meanwhile, until now, most of the optical studies on the $CsPbBr_3$ QDs have been focusing on the linear part. In comparison, their corresponding nonlinear optical properties are scarcely discussed. In contrast to linear absorption and emission, the multiphoton feature possesses several merits including a large penetration depth, high spatial resolution, and

[a]*State Key Laboratory of High Power Semiconductor Lasers, School of Science, Changchun University of Science and Technology, 7089 Wei-Xing Road, Changchun 130022, P. R. China. E-mail: zpweicust@126.com*

[b]*Department of Electrical and Electronic Engineering, South University of Science and Technology of China, Shenzhen, Guangdong 518055, P. R. China. E-mail: chen.r@sustc.edu.cn*

[c]*College of Physics and Energy, Shenzhen University, Shenzhen, Guangdong 518060, P. R. China*

†Electronic supplementary information (ESI) available. See DOI: 10.1039/c8nr07256f

little damage to the targeted samples.[6,21–24] In addition, in the perovskite $CsPbBr_3$ it has been found that its triplet states are active.[25] The triplet states play a key role in optical limiting (OL) performance, and the capability of OL depends on the photo-generation of highly absorbing the triplet states.[26,27] Thus, the nonlinear optical applications are one of the most important aspects of the $CsPbBr_3$ QDs, and their stability requirements are more crucial due to higher excitation. Therefore, new strategies are needed to improve the optical stabilities of $CsPbBr_3$ QDs.

In this work, hydrophobic zeolite was proposed for $CsPbBr_3$ QDs to effectively depress their optical degradation. It was found that such hydrophobic zeolite provides an effective hydrophobic surface for $CsPbBr_3$ QDs to prevent the influence of polar water molecules. In addition, the enlarged surface tension induced by hydrophobic zeolite can improve the dispersion of the $CsPbBr_3$ QDs. It is necessary to mention that our modification does not affect the light extraction efficiency compared to the encapsulation method. Thus, the modified perovskite can be used as a light emitting material like phosphor. As a result, the $CsPbBr_3$ QDs demonstrate very high optical, temperature and nonlinear OL stability, which was verified by systematic optical measurements. This strategy is universal to other halide perovskite materials, and it also opens the window of perovskite-based multifunctional composites (replacing other superhydrophobic materials, luminescent materials, and so on). In addition, it would be of importance regarding both fundamental physics interest and practical multiphoton and multifunctional applications.

## 2 Results and discussion

In Fig. 1a and b are the schematics of $CsPbBr_3$ QDs without and with the hydrophobic zeolite. As shown in Fig. 1a, the $CsPbBr_3$ QDs are directly spin coated on Si, while in Fig. 1b, most of the $CsPbBr_3$ QDs are distributed on the outer surface of hydrophobic zeolite. It is very clear to see that a part of the $CsPbBr_3$ QDs without hydrophobic zeolite collapses while the $CsPbBr_3$ QDs with hydrophobic zeolite have a completely neat structure. As mentioned above, all-inorganic perovskite $CsPbBr_3$ QDs are very sensitive to water and moisture.[10] In the schematic diagram shown in Fig. 1a, it can be seen that the Cs ions occupy the vertices of cubes, while Pb and Br ions assemble into octahedra ($PbBr_6^{4-}$) in the center of the framework formed by Cs. These materials degrade because they are highly ionic structures and therefore dissociate in polar solvents, such as water,[8,9] and then the $CsPbBr_3$ QDs will pile up and a part of their structure will collapse and regrow during the spin-cast procedure before the hydrophobic layer is coated, which are shown in Fig. 1a. These properties will limit its practical applications based on this new kind of functional material. To solve the problem, in this paper a kind of relative hydrophobic zeolite was proposed to enhance the hydrophobicity and dispersibility of $CsPbBr_3$ QDs, and some natural water-barriers can be formed that keeps $CsPbBr_3$ QDs away from water and moisture, as shown in Fig. 1b. Therefore, both the moisture-induced structural and optical degeneration in $CsPbBr_3$ QDs can be solved.

Three kinds of commercially available zeolites are chosen for discussion in this paper, which are named SBA-15, MCM-41 and SAPO-34. The water contact angles (CAs)[28,29] of the three zeolites were measured to be 0°, 58° and 96°, respectively, and the pictures are shown in Fig. S1.† Hydrophobicity implies a water contact angle above 90°,[30] so that this result indicates that only SAPO-34 is the hydrophobic one among these three zeolites, and we have confirmed in our experiments below that hydrophobic zeolites can improve the optical properties of perovskite.

To investigate the morphologies of $CsPbBr_3$ QDs, scanning electron microscopy (SEM) and high-resolution transmission electron microscopy (HRTEM) characterization studies were

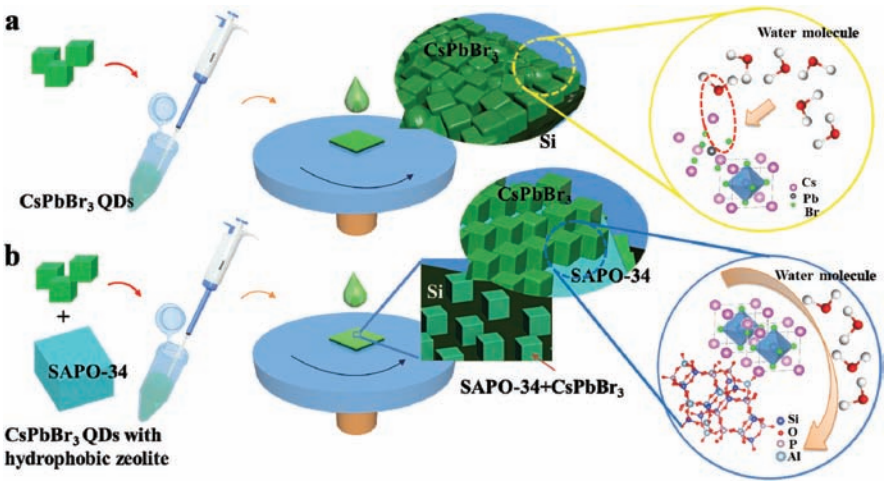


Fig. 1 The synthesis process of hybrid luminescent materials of $CsPbBr_3$ QDs with hydrophobic zeolite and the mechanism of forming natural water-barriers to maintain a well-defined crystalline structure.

carried out and are shown in Fig. 2. From the SEM images in Fig. 2a, it can be clearly seen that the $CsPbBr_3$ QDs are cubic in shape with diameters of about 10 nm, while the zeolites demonstrate cuboid or cubic shape with about 2–3 μm length. Before the TEM measurements, the $CsPbBr_3$ QDs are respectively mixed with different zeolites and then stored at room temperature for about two weeks. Detailed procedures can be found in the Experimental sections. For convenient discussion, the $CsPbBr_3$ QDs without and with zeolites (mixtures of SBA-15-zeolite-$CsPbBr_3$ QDs, MCM-41-zeolite-$CsPbBr_3$ QDs and SAPO-34-zeolite-$CsPbBr_3$ QDs) are named 1#-WOZ, 2#-S15, 3#-M41 and 4#-S34 QDs, respectively. In the TEM images of Fig. 2b, it can be seen that all the samples with zeolites are well distributed around the zeolites, which is due to the organic ligands on the surface of $CsPbBr_3$ QDs and the lipophilicity of zeolites.[10] Although the QDs are all distributed around the zeolites, it can be seen from the HRTEM images of Fig. 2c that different hydrophobic zeolites have different influences on the morphologies of the $CsPbBr_3$ QDs. It is shown that both the 1#-WOZ and 2#-S15 samples have blurred shapes with a high degree of aggregation, while the 3#-M41 and 4#-S34 samples demonstrate clear shapes and the QDs are well separated from each other. This indicates that the hydrophobic zeolite is beneficial for the better dispersion of $CsPbBr_3$ QDs and they will have a more uniform size and bigger diameter. Furthermore, this is also confirmed by the histogram of the size distribution of the samples in Fig. S2.† The diameter of 1#-WOZ distributes in a relatively wider range of 6–13 nm with an average diameter of 9.55 nm, while the diameters of the 2#-S15 to 4#-S34 samples distribute in a relatively narrower range and a bigger size. Here, the change of QD size is caused by the subsequent dissociation due to the influence of water. The insets of Fig. 2c are close-up TEM images of one single $CsPbBr_3$ QD and its corresponding Fourier transform (FFT) patterns. Clear lattice fringes with a lattice plane distance of ~0.58 nm in all samples can be observed. Strong and bright diffraction spot arrays indicate that the QDs possess a well-defined crystalline structure.[3,31] The distance of the diffraction spot arrays of the FFT patterns is ~1.75 1 $nm^{-1}$, which is consistent with the lattice plane distance. According to different synthesis temperatures and the surface energies (related to the distortion of the $PbBr_6^{4-}$ octahedra), $CsPbBr_3$ QDs are known to have orthorhombic, tetragonal, and cubic crystal structures.[2,8,9,31] The cubic phase is different from orthorhombic and tetragonal phases. However, it may difficult to distinguish the latter two based on our obtained information. Nevertheless, it is needed to mention that the crystal structure will not be influenced through modification by the hydrophobic zeolite, and it is not the focus of our work. It is found that all $CsPbBr_3$ QDs in this paper are the same phase at room temperature (about two weeks after being synthesized), which is also confirmed by the selected area electron diffraction (SAED) patterns in Fig. S3 and Table S1.† And the powder X-ray diffraction (XRD) data (Fig. S4†) also show that these four samples are in the same phase at room temperature.

Room temperature photoluminescence (RTPL) spectra of $CsPbBr_3$ QDs without and with zeolites are shown in Fig. 3. The PL peaks were found at 514.4, 515.69, 516.29 and 517.59 nm for 1#-WOZ, 2#-S15, 3#-M41 and 4#-S34 QDs, respectively. Optical absorption spectra of the zeolites are shown in Fig. S5,† indicating that all the zeolites have no absorption in the visible region and the emissions only come from the $CsPbBr_3$ QDs. It can be seen that the values of the PL peak of the samples with zeolites (the inset) are redshifted gradually, which may be caused by quantum confinement effects. The average radius of $CsPbBr_3$ QDs is estimated using the following eqn (1) by the quantum confinement effect:[32]

$$E(R) = E_g + \frac{\hbar^2\pi^2}{2R}\left(\frac{1}{m_e^*} + \frac{1}{m_h^*}\right) - \frac{1.8e^2}{\varepsilon R} \quad (1)$$

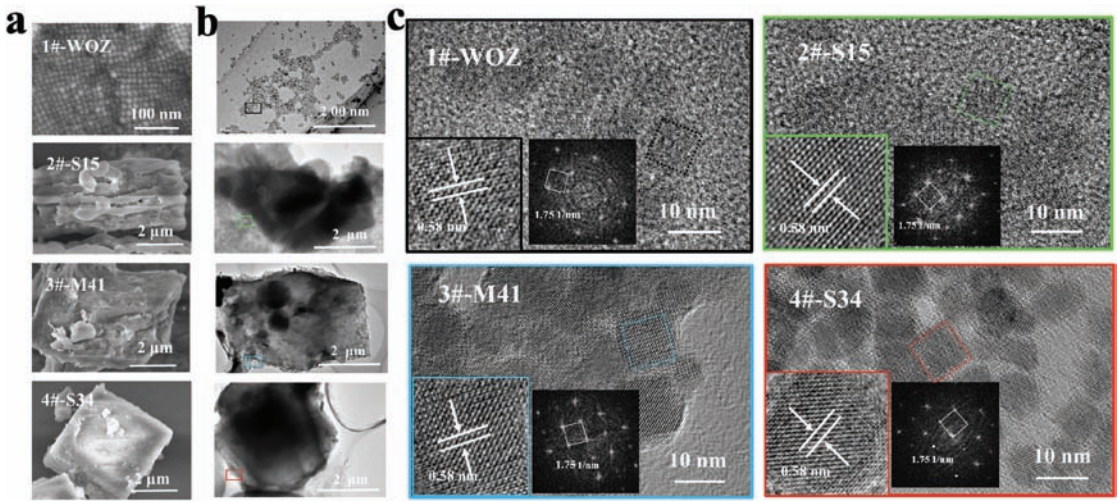


Fig. 2 a. SEM images of the QDs and SBA-15, MCM-41, and SAPO-34 zeolites. b. TEM images of the $CsPbBr_3$ QDs without and with different zeolites. c. HRTEM images of 1#-WOZ to 4#-S34 samples, and insets are close-up TEM images and Fourier transform patterns.

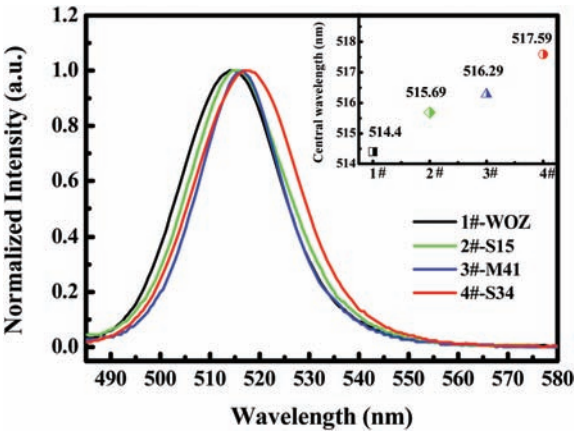


Fig. 3 Room temperature PL of the $CsPbBr_3$ QDs without and with different zeolites. Inset is the PL peak positions of the samples.

where $E(R)$ is the effective band gap energy, $E_g$ is the band gap energy of bulk $CsPbBr_3$ semiconductor ($E_g$ = 2.3 eV),[33,34] and $R$ is the radius of the $CsPbBr_3$ QDs. The second term is the kinetic energies of the electron and hole that increase as the particle size decreases. The third term is the screened Coulomb interaction which stabilizes the electron–hole pair. The $m_e^*$ and $m_h^*$ are the effective mass of the electron and hole, which are found to be $0.15m_e$ and $0.14m_e$ at room temperature.[9,32] The average radii of $CsPbBr_3$ QDs formed in 1#-WOZ, 2#-S15, 3#-M41 and 4#-S34 QDs were found to be 5.38, 5.53, 5.61 and 5.78 nm, respectively. This trend is consistent with the histogram of the size distribution, and also confirmed that the hydrophobic zeolite contributes to the good dispersion of $CsPbBr_3$ QDs.

Internal quantum efficiency (IQE) is important for luminescent materials and can be used to analyze the degree of defects in different $CsPbBr_3$ QD samples.[35] It can be determined from power-dependent PL measurements (Fig. S6† and Fig. 4). IQE is related to the nonradiative recombination $An$ and bimolecular radiative recombination $Bn^2$ (the excitation power used during our experiment is lower than that used in the literature;[35] therefore, the Auger nonradiative recombination is ignored in this paper), where $A$ and $B$ are the respective recombination coefficients and $n$ is the carrier concentration. Thus, the generation rate and the IQE at steady state can be estimated using the following eqn (2) and (3):[35]

$$G = R_{\text{total}} = An + Bn^2 \tag{2}$$

$$IQE = \frac{Bn^2}{An + Bn} = \frac{Bn^2}{G} \tag{3}$$

and the integrated PL intensity can be estimated as eqn (4)

$$I_{\text{PL}} = \eta Bn^2 \tag{4}$$

where $\eta$ is a constant determined by the volume of the excited active region and the total collection efficiency of luminescence. By eliminating $n$ in eqn (2) and (4), the generation rate in terms of integrated PL intensity can be expressed as:

$$G = \frac{A}{\sqrt{B\eta}} + \frac{1}{\eta} I_{PL} \tag{5}$$

The connection between theory and experiment is completed by noting that the generation rate can be separately calculated from experimental parameters using

$$G = \frac{P_{laser}(1-R)\alpha l}{(A_{spot} l h\nu)} = \frac{P_{laser}(1-R)\alpha}{A_{spot} h\nu} \tag{6}$$

where $P_{\text{laser}}/A_{\text{spot}}$ is the power density of the laser ranging from 0.4 to 26 W $cm^{-2}$, $R$ is the Fresnel reflection (18%), $h\nu$ is the photon energy of the laser (2.774 eV), and $\alpha$ is the linear absorption coefficient of $CsPbBr_3$ at 447 nm ($0.6 \times 10^5$ $cm^{-1}$).[36] The value of $G$ for the four $CsPbBr_3$ samples should be the same or similar under the same measured conditions; however, the nonradiative recombination effects will make them have different IQE values. Therefore, using eqn (5) [eliminating $I_{\text{PL}}$ using eqn (2)] and eliminating a value of $B$ at room temperature of $1 \times 10^{-10}$ $cm^3$ $s^{-1}$,[37,38] the IQE and the nonradiative recombination coefficient $A$ can be obtained. From Fig. 4a, it can be seen that the carrier concentration of $CsPbBr_3$ QDs in this paper is about $\sim 10^{17}$ $cm^{-3}$. However, in Fig. 4b, the most hydrophobic 4#-S34 sample demonstrates the highest $I_{\text{PL}}$ under the same value of $G$. It implies that the nonradiative recombination effect in the 4#-S34 sample may be very low. In Fig. 4c and d, the values of the nonradiative recombination coefficient $A$ and the IQE of the samples are provided. The hydrophobic 4#-S34 sample demonstrates the lowest value of $A$ and the highest value of the IQE (80.7% at 3.52 W $cm^{-2}$), indicating the 4#-S34 sample possesses the lowest defect level. Therefore, the hydrophobic zeolite is conducive in maintaining a better-defined crystalline structure in $CsPbBr_3$ QDs, and will give rise to a very strong competitive advantage regarding its stability in performance.

In order to discuss their optical stability, temperature dependent PL (TDPL) and the measurements of photostability were carried out. As shown in Fig. 5a and b, pseudo-color maps of the TDPL spectra and the normalized intensity of PL emission with temperature from 10–300 K were plotted. From Fig. 5a, the full width at half maximum (FWHM) of the 3#-M41 and 4#-S34 samples are narrower than that of the 2#-S15 sample. In addition, compared with the 2#-S15 and 3#-M41 samples, the most hydrophobic 4#-S34 sample possesses a higher intensity. Although the 1#-WOZ sample has higher intensity than the 4#-S34 sample in the low temperature range, its PL intensity decreases more than 2 orders of magnitude from 10 to 300 K, while the emission intensity from the 4#-S34 sample changes only about 2.5 times under the identical temperature range. Therefore, it implies that the hydrophobic zeolite is conducive to the emission of $CsPbBr_3$ QDs, and can greatly suppress the surface trapping and nonradiative recombination process, which enables broad emission.[39] This result is consistent with power-dependent PL measurements, and

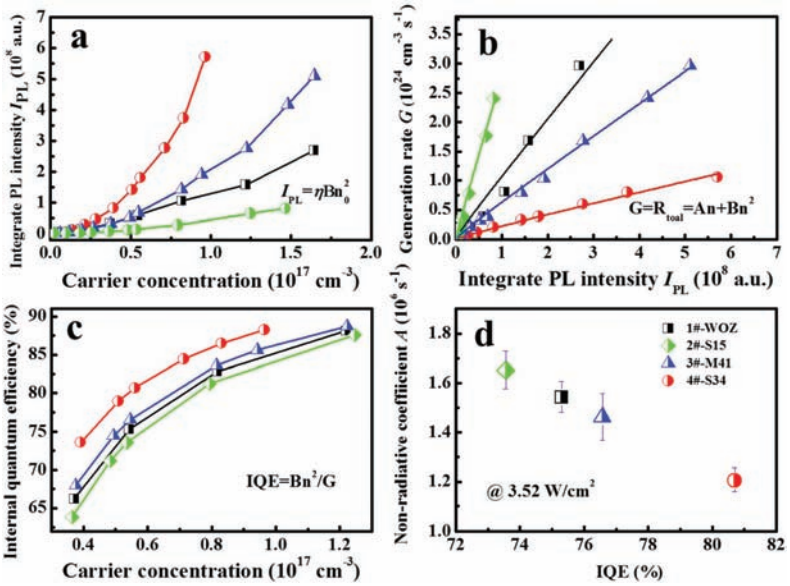


Fig. 4 a. The experimental results for the integrated PL and carrier concentration. b. Generation rate $G$ as a function of $I_{PL}$ obtained using eqn (4) and (6). c. Internal quantum efficiency (IQE) as a function of carrier concentration. d. Nonradiative coefficient $A$ as a function of IQE.

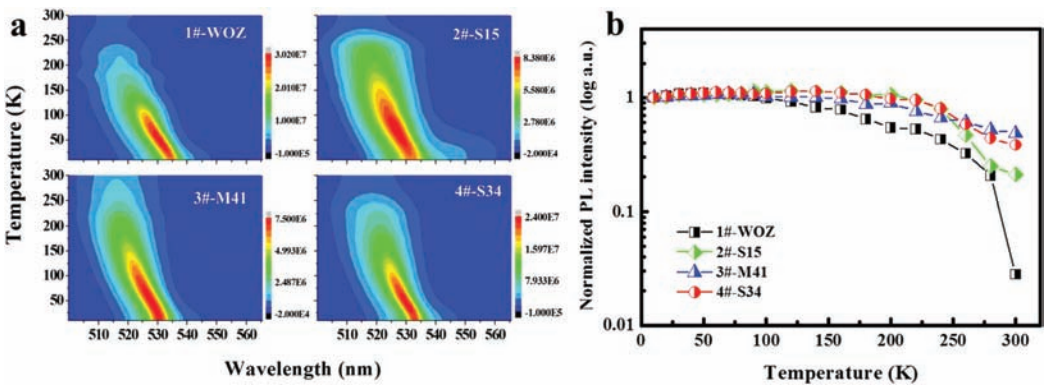


Fig. 5 Pseudo-color maps of temperature-dependent PL spectra of the $CsPbBr_3$ QDs without and with different zeolites. b. Normalized intensity of PL emission with increased temperatures.

such kinds of composite materials should be very useful for high-performance optoelectronic device applications.[40]

The measurements of photostability were carried out under strong and continuous laser (447 nm, 3.52 W cm$^{-2}$) irradiation. All the samples were dispersed on a Si substrate and exposed to laser light directly at room temperature, and the measurement period ranged from 0 to 45 days. The samples were stored in the surrounding environment, and the measurement was tested once every day. In Fig. 6, the intensity of the emission of the 1#-WOZ sample decreased to 0.1% after 45 days, while the intensity of the samples with zeolite remained almost constant, especially the 4#-S34 sample. An industrial camera (Point Grey, Canada) was used to collect digital photographs of the luminescence of the samples, which clearly shows the trend of the optical degradation during testing, as shown in the insets of Fig. 6. From the

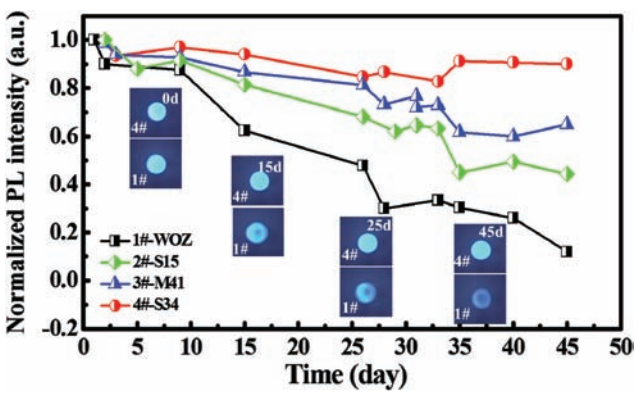


Fig. 6 Photostabilities of the $CsPbBr_3$ QDs without and with different zeolites. The inset is the digital photographs collected using an industrial camera (Point Grey).

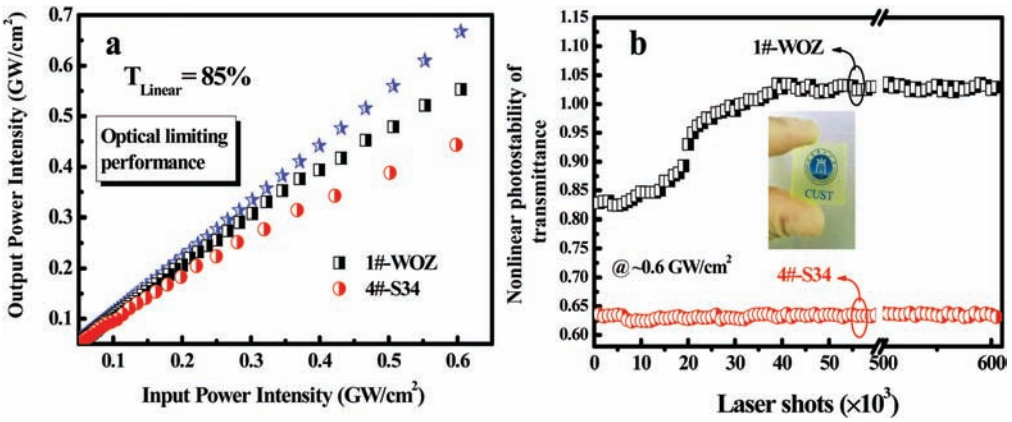


Fig. 7 a. The OL performance of 1#-WOZ and 4#-S34 samples. b. Nonlinear photostability of the materials. The inset is the image of the transparent sample.

figures, it can be seen that the optical degradation of the 1#-WOZ sample is very serious, while the 4#-S34 sample maintains its brightness after 45 days. Therefore, it indicates that zeolites with stronger hydrophobic effect are able to effectively improve the optical degradation in $CsPbBr_3$ QDs and give superstability under continuous pumping.

The ultra-stable $CsPbBr_3$ QDs modified by hydrophobic zeolites enable the investigation of the nonlinear optical property of the materials. Fig. 7a and b show the OL performance of the 1#-WOZ and 4#-S34 samples and their nonlinear photostabilities. The blue stars line represents the linear transmittance, which corresponds to no nonlinear effect in the $CsPbBr_3$. It is the slope of the normal transmittance of $CsPbBr_3$ under low power femtosecond laser irradiation. The inset is the digital photograph of the 4#-S34 sample, which indicates the uniformity and transparency of the film. Femtosecond pulses (100 fs and 1 kHz) at 720 nm were used as the OL excited source. Detailed procedures can be found in the Experimental sections. The two-photon absorption (TPA) can give access to large transient absorption effects, which is similar to the carrier transmission path of reverse saturable absorption.[26] As shown in Fig. 7a, both the 1#-WOZ and 4#-S34 samples show OL performance. Considering that the linear absorption beyond 480 nm was absent for the studied $CsPbBr_3$ QDs, the observed OL was thus attributed to TPA. Based on the results of fitting open-aperture *Z*-scans (Fig. S8†), the TPA coefficients of 1#-WOZ and 4#-S34 samples are determined to be 2.79 and 3.01 cm per MW, respectively.[41] In addition, from Fig. 7b, it can be seen that the nonlinear photostability of the 4#-S34 sample has been improved, while the 1#-WOZ sample is damaged in such a high excited source at 0.6 GW per $cm^2$. This is because that a part structure of the 1#-WOZ sample has been destroyed by moist surroundings and its defect states will hinder the photo-generation of transient absorption effects. It is needed to emphasise that for nonlinear multiphoton optical limiting, extremely high-power femtosecond pulses and a thin sample for better transmittance are usually used. To characterize the optical stability, the time of the sample under intensive laser will be counted, as shown in Fig. 7 (the measurement is sustained for about 10 min, identically $10^5$ laser shots, and the bare sample was destroyed after 45 seconds when the transmittance is larger than 1). This is the general and reasonable measurement time-scale that has been reported.[41] Therefore, this measurement can largely demonstrate that the zeolite modified $CsPbBr_3$ sample has better photostability. The nonlinear multiphoton optical limiting values for different materials are shown in Table 1. There are different inorganic materials including II–VI semiconductor nanocrystals,[42,43] II–VI core–shell semiconductors,[44] 2D transition metal dichalcogenide mono-/few-layers,[45] 2D/3D perovskite films,[45] perovskite single crystals,[46] and $CsPbBr_3$ QDs.[47] It can be clearly seen that all of these nanomaterials are considered to possess nonlinear optical absorption effects and the nonlinear multiphoton optical limiting transmittance values are about 70%–90%. In our work, compared to the $CsPbBr_3$ QDs sample, the hydrophobic zeolite modified sample has maintained the nonlinear photostability for more than 10 times longer in time, and reduced by ~25% in transmittance, which are a very good result in the field of nonlinear multiphoton optical limiting. This is the best result in the current research field. Therefore, the nanocomposite of the $CsPbBr_3$ QDs with the hydrophobic zeolite possesses a low dissociation level that gives rise to improvement of the optical stability in terms of temperature and time, and for the benefit of its practical applications.

# 3 Experimental section

## 3.1 Preparation of zeolite-perovskite luminescent composites

The synthetic procedure of $CsPbBr_3$ is similar to what was reported previously.[3,9,10] All the chemicals were purchased from Aladdin and used without further purification. Subsequently, the $CsPbBr_3$ QDs were dispersed into hexane with a concentration of ~50 mg $mL^{-1}$. For the preparation of hybrid luminescent materials of $CsPbBr_3$ QDs with the hydrophobic zeolite, 0.2 mL of the green $CsPbBr_3$ QDs (~50 mg

Table 1 Nonlinear multiphoton optical limiting for different materials

| Material | Laser | Thickness | Nonlinear absorption | *T*% | Ref. |
|---|---|---|---|---|---|
| ZnO nanoparticles | 700 nm, 130 fs | 5–10 nm | SA/TPA[a,b] | 80% | 36 and 37 |
| ZnO nanoparticles | 800 nm 100 fs | 5–10 nm | TPA | N/A | 36 and 37 |
| CdS nanocrystals | 140 fs, 1 kHz | 1.8 μm | SA/TPA | 83% | 36 and 38 |
| CdTe/CdS QDs | 515 nm, 340 fs, 1 kHz | N/A | SA/TPA | 84% | 39 |
| $WS_2$ monolayer | 800 nm, 40 fs, 1 kHz | 0.75 nm | TPA | 92.21% | 36 and 40 |
| $WS_2$ multilayer | 800 nm, 40 fs, 1 kHz | 20 nm | TPA | 88.98% | 36 and 40 |
| $MAPbI_3$ film | 800 nm, 100 fs, 1 kHz | 1 μm | SA | 73% | 36 and 40 |
| $MAPbBr_3$ film | 800 nm, 100 fs, 1 kHz | 0.38 μm | SA/TPA | 76% | 36 and 40 |
| $MAPbBr_3$ single crystals | 1064 nm, 30 ps, 50 Hz | N/A | SA/TPA | ~90% | 41 |
| $CsPbBr_3$ single crystal | 1000 nm, 30 ps, 50 Hz | N/A | SA/TPA | ~90% | 41 |
| $CsPbBr_3$ QDs | 515 nm, ~340 fs, 1 kHz | N/A | SA/TPA | 93% | 42 |
| $CsPbBr_3$ QDs film | 720 nm, 100 fs, 1 kHz | 20–50 nm | SA/TPA | 85% | This work |
| $CsPbBr_3$ QDs-zeolite film | 720 nm, 100 fs, 1 kHz | 20–50 nm | SA/TPA | 62% | This work |

[a] TPA, two-photon absorption. [b] SA, saturable absorption.

$mL^{-1}$ in hexane) was mixed with 5 mg of zeolite powder. The resulting solution was stirred for 10 min. Afterward, the mixture was spin-cast on the Si substrate at 1000 revolutions per minute (rpm) for 30 s in air followed by 500 rpm for 5 s. This procedure was repeated multiple (2–3) times to build up 100–400 nm thick $CsPbBr_3$ QD films and 2–3 μm zeolite-$CsPbBr_3$ QD layer.

### 3.2 Characterization

The microstructures of the products were investigated using field emission scanning electron microscope (FESEM) (Hitachi S-4800) equipped with an energy-dispersive X-ray (EDX) spectrometer (GENE SIS 2000 XMS 60S, EDAX, Inc.). The particle size and shape of the samples were characterized through transmission electron microscopy (TEM) with an FEI Tecnai G2 F20 microscope operated at 200 kV. TEM grids were prepared by dropping a dilute colloidal solution of QDs in hexane onto the carbon coated copper grids. The room temperature photoluminescence (RTPL) spectra were obtained using a Horiba iHR550 spectrometer at an excitation wavelength of 447 nm, working with a 1200 g $mm^{-1}$ grating. The power of the excitation laser is 0.1 mW, and the spot size is ~0.002 $cm^2$. The temperature dependent PL (TDPL) and photostability measurements are carried out at 10–300 K in a vacuum chamber, and the temperature was controlled using a conventional backscattering geometry in a closed-cycle He cryostat.

### 3.3 Nonlinear optics and optical limiting performance measurement

For the preparation of the solid film, the samples were drop-casted on a pre-cleaned 1 mm thick and 10 mm length square quartz substrate. The spin-cast procedure was performed at 5000 rpm for 30 s followed by 1000 rpm for 5 s. A femtosecond amplified laser system was adopted as the laser source. The pulse-width and repetition rate were 100 fs and 1 kHz, respectively. The laser wavelength at 720 nm was used as the two-photon excited source. For the *Z*-scan measurements, the laser beam was divided into two parts by a beam splitter. One acted as the reference (the open aperture), and the other one was focused onto the film by a circular lens (focus length: 50 cm) and detected by a CCD camera. The sample was controlled by a step motor travelling along the laser beam back and forth.

## 4 Conclusions

In conclusion, hybrid luminescent materials of $CsPbBr_3$ QDs with the hydrophobic zeolite were created in this paper. The QDs can be simply synthesized and are suitable for industrial manufacturing. The hydrophobic zeolite can provide an effective hydrophobic surface for $CsPbBr_3$ QDs to prevent the influence of polar water molecules, and its' enlarged surface tension can improve the dispersion of the $CsPbBr_3$ QDs. Thus, the $CsPbBr_3$ QDs give rise to improved temperature-insensitive and superlinear and nonlinear optical stability. This strategy is universal to other halide perovskite materials, and it also opens the window to perovskite-based multifunctional composites and would be of importance regarding both fundamental physics interest and practical multiphoton and multifunctional applications.

## Conflicts of interest

There are no conflicts to declare.

## Acknowledgements

This work is supported by the National Natural Science Foundation of China (11574130, 61404009, 61474010, 61574022, 61504012, 61674021, 11404219, and 11674038) and the Developing Project of Science and Technology of Jilin Province (20160519007JH, 20160520117JH, 20160101255JC, 20160204074GX, 20170520117JH, and 20170520118JH) and Foundation of NANO X (18JG01). R. C. acknowledges the National 1000 plan for young talents and the Shenzhen Science and Technology Innovation Committee (Projects No.

 

KQJSCX20170726145748464, JCYJ20150930160634263 and KQTD2015071710313656).

## References


1 J. Huang, Y. Yuan, Y. Shao and Y. Yan, *Nat. Rev. Mater.*, 2017, **2**, 17042.
2 A. Swarnkar, A. R. Marshall, E. M. Sanehira, B. D. Chernomordik, D. T. Moore, J. A. Christians, T. Chakrabarti and J. M. Luther, *Science*, 2016, **354**, 92–95.
3 Z. Shi, Y. Li, Y. Zhang, Y. Chen, X. Li, D. Wu, T. Xu, C. Shan and G. Du, *Nano Lett.*, 2017, **17**, 313–321.
4 Y. Xu, Q. Chen, C. Zhang, R. Wang, H. Wu, X. Zhang, G. Xing, W. W. Yu, X. Wang, Y. Zhang and M. Xiao, *J. Am. Chem. Soc.*, 2016, **138**, 3761–3768.
5 F. Zhang, H. Zhong, C. Chen, X.-g. Wu, X. Hu, H. Huang, J. Han, B. Zou and Y. Dong, *ACS Nano*, 2015, **9**, 4533–4542.
6 Y. Wang, X. Li, X. Zhao, L. Xiao, H. Zeng and H. Sun, *Nano Lett.*, 2016, **16**, 448–453.
7 N. Yantara, S. Bhaumik, F. Yan, D. Sabba, H. A. Dewi, N. Mathews, P. P. Boix, H. V. Demir and S. Mhaisalkar, *J. Phys. Chem. Lett.*, 2015, **6**, 4360–4364.
8 C. C. Stoumpos, C. D. Malliakas, J. A. Peters, Z. F. Liu, M. Sebastian, J. Im, T. C. Chasapis, A. C. Wibowo, D. Y. Chung, A. J. Freeman, B. W. Wessels and M. G. Kanatzidis, *Cryst. Growth Des.*, 2013, **13**, 2722–2727.
9 L. Protesescu, S. Yakunin, M. I. Bodnarchuk, F. Krieg, R. Caputo, C. H. Hendon, R. X. Yang, A. Walsh and M. V. Kovalenko, *Nano Lett.*, 2015, **15**, 3692–3696.
10 J. Li, L. Xu, T. Wang, J. Song, J. Chen, J. Xue, Y. Dong, B. Cai, Q. Shan, B. Han and H. Zeng, *Adv. Mater.*, 2017, **29**, 1603885.
11 F. Palazon, Q. A. Akkerman, M. Prato and L. Manna, *ACS Nano*, 2016, **10**, 1224–1230.
12 S. Ye, J.-Y. Sun, Y.-H. Han, Y.-Y. Zhou and Q.-Y. Zhang, *ACS Appl. Mater. Interfaces*, 2018, **10**, 24656–24664.
13 S. Hou, Y. Guo, Y. Tang and Q. Quan, *ACS Appl. Mater. Interfaces*, 2017, **9**, 18417–18422.
14 S. N. Raja, Y. Bekenstein, M. A. Koc, S. Fischer, D. Zhang, L. Lin, R. O. Ritchie, P. Yang and A. P. Alivisatos, *ACS Appl. Mater. Interfaces*, 2016, **8**, 35523–35533.
15 H. Huang, B. Chen, Z. Wang, T. F. Hung, A. S. Susha, H. Zhong and A. L. Rogach, *Chem. Sci.*, 2016, **7**, 5699–5703.
16 A. Loiudice, S. Saris, E. Oveisi, D. T. L. Alexander and R. Buonsanti, *Angew. Chem., Int. Ed.*, 2017, **56**, 10696–10701.
17 L. N. Quan, R. Quintero-Bermudez, O. Voznyy, G. Walters, A. Jain, J. Z. Fan, X. Zheng, Z. Yang and E. H. Sargent, *Adv. Mater.*, 2017, **29**, 1605945.
18 Y. Wu, Y. Wei, Y. Huang, F. Cao, D. J. Yu, X. M. Li and H. B. Zeng, *Nano Res.*, 2017, **10**, 1584–1594.
19 H. C. Wang, S. Y. Lin, A. C. Tang, B. P. Singh, H. C. Tong, C. Y. Chen, Y. C. Lee, T. L. Tsai and R. S. Liu, *Angew. Chem., Int. Ed.*, 2016, **55**, 7924–7929.
20 L. N. Quan, R. Quintero-Bermudez, O. Voznyy, G. Walters, A. Jain, J. Z. Fan, X. Zheng, Z. Yang and E. H. Sargent, *Adv. Mater.*, 2017, **29**, 1605945.
21 Y. Wang, V. D. Ta, Y. Gao, T. C. He, R. Chen, E. Mutlugun, H. V. Demir and H. D. Sun, *Adv. Mater.*, 2014, **26**, 2954–2961.
22 G. S. He, P. P. Markowicz, T. C. Lin and P. N. Prasad, *Nature*, 2002, **415**, 767–770.
23 Y. Wang, X. Yang, T. C. He, Y. Gao, H. V. Demir, X. W. Sun and H. D. Sun, *Appl. Phys. Lett.*, 2013, **102**, 021917.
24 W. Chen, S. Bhaumik, S. A. Veldhuis, G. Xing, Q. Xu, M. Grätzel, S. Mhaisalkar, N. Mathews and T. C. Sum, *Nat. Commun.*, 2017, **8**, 15198.
25 M. A. Becker, R. Vaxenburg, G. Nedelcu, P. C. Sercel, A. Shabaev, M. J. Mehl, J. G. Michopoulos, S. G. Lambrakos, N. Bernstein, J. L. Lyons, T. Stoferle, R. F. Mahrt, M. V. Kovalenko, D. J. Norris, G. Raino and A. L. Efros, *Nature*, 2018, **553**, 189–193.
26 C. W. Spangler, *J. Mater. Chem.*, 1999, **9**, 2013–2020.
27 W. Wei, T. He, X. Teng, S. Wu, L. Ma, H. Zhang, J. Ma, Y. Yang, H. Chen, Y. Han, H. Sun and L. Huang, *Small*, 2012, **8**, 2271–2276.
28 K. Lum, D. Chandler and J. D. Weeks, *J. Phys. Chem. B*, 1999, **103**, 4570–4577.
29 L. Feng, S. Li, Y. Li, H. Li, L. Zhang, J. Zhai, Y. Song, B. Liu, L. Jiang and D. Zhu, *Adv. Mater.*, 2002, **14**, 1857–1860.
30 K.-Y. Law, *J. Phys. Chem. Lett.*, 2014, **5**, 686–688.
31 S. Sun, D. Yuan, Y. Xu, A. Wang and Z. Deng, *ACS Nano*, 2016, **10**, 3648–3657.
32 B. Ai, C. Liu, Z. Deng, J. Wang, J. Han and X. Zhao, *Phys. Chem. Chem. Phys.*, 2017, **19**, 17349–17355.
33 J. Liang, C. Wang, Y. Wang, Z. Xu, Z. Lu, Y. Ma, H. Zhu, Y. Hu, C. Xiao, X. Yi, G. Zhu, H. Lv, L. Ma, T. Chen, Z. Tie, Z. Jin and J. Liu, *J. Am. Chem. Soc.*, 2016, **138**, 15829–15832.
34 M. Sebastian, J. A. Peters, C. C. Stoumpos, J. Im, S. S. Kostina, Z. Liu, M. G. Kanatzidis, A. J. Freeman and B. W. Wessels, *Phys. Rev. B: Condens. Matter Mater. Phys.*, 2015, **92**, 235210.
35 Q. Dai, M. F. Schubert, M. H. Kim, J. K. Kim, E. F. Schubert, D. D. Koleske, M. H. Crawford, S. R. Lee, A. J. Fischer, G. Thaler and M. A. Banas, *Appl. Phys. Lett.*, 2009, **94**, 111109.
36 J. De Roo, M. Ibanez, P. Geiregat, G. Nedelcu, W. Walravens, J. Maes, J. C. Martins, I. Van Driessche, M. V. Kovalenko and Z. Hens, *ACS Nano*, 2016, **10**, 2071–2081.
37 E. F. Schubert, in *Light-emitting diodes*, Cambridge University Press, Cambridge, New York, 2006, ch. 2, pp. 27–31, DOI: 10.1017/CBO9780511790546.
38 H. Y. Ryu, K. H. Ha, J. H. Chae, K. S. Kim, J. K. Son, O. H. Nam, Y. J. Park and J. I. Shim, *Appl. Phys. Lett.*, 2006, **89**, 171106.
39 R. Chen, Q. L. Ye, T. He, V. D. Ta, Y. Ying, Y. Y. Tay, T. Wu and H. Sun, *Nano Lett.*, 2013, **13**, 734–739.
40 J. Y. Sun, F. T. Rabouw, X. F. Yang, X. Y. Huang, X.-P. Jing, S. Ye and Q.-Y. Zhang, *Adv. Funct. Mater.*, 2017, **27**, 1704371.

41 W. Liu, J. Xing, J. Zhao, X. Wen, K. Wang, P. Lu and Q. Xiong, *Adv. Opt. Mater.*, 2017, **5**, 1601045.
42 E. V. Chelnokov, N. Bityurin, I. Ozerov and W. Marine, *Appl. Phys. Lett.*, 2006, **89**, 171119.
43 J. He, J. Mi, H. Li and W. Ji, *J. Phys. Chem. B*, 2005, **109**, 19184–19187.
44 J. Li, S. Zhang, H. Dong, Y. Ma, B. Xu, J. Wang, Z. Cai, Z. Chen and L. Zhang, *Part. Part. Syst. Charact.*, 2016, **34**, 1600193.
45 S. Zhang, N. Dong, N. McEvoy, M. O'Brien, S. Winters, N. C. Berner, C. Yim, Y. Li, X. Zhang, Z. Chen, L. Zhang, G. S. Duesberg and J. Wang, *ACS Nano*, 2015, **9**, 7142–7150.
46 F. O. Saouma, D. Y. Park, S. H. Kim, M. S. Jeong and J. I. Jang, *Chem. Mater.*, 2017, **29**, 6876–6882.
47 F. O. Saouma, C. C. Stoumpos, M. G. Kanatzidis, Y. S. Kim and J. I. Jang, *J. Phys. Chem. Lett.*, 2017, **8**, 4912–4917.